

Experimental simulation of quantum graphs by microwave networks

Oleh Hul¹, Szymon Bauch¹, Prot Pakoński², Nazar Savytskyi¹,
Karol Życzkowski^{2,3}, and Leszek Sirko¹

¹*Institute of Physics, Polish Academy of Sciences,
Aleja Lotników 32/46, 02-668 Warszawa, Poland*

²*Instytut Fizyki im. Smoluchowskiego, Uniwersytet Jagielloński,
ul. Reymonta 4, 30-059 Kraków, Poland*

³*Center for Theoretical Physics, Polish Academy of Sciences,
Aleja Lotników 32/46, 02-668 Warszawa, Poland*

(Dated: February 3, 2004)

Abstract

We present the results of experimental and theoretical study of irregular, tetrahedral microwave networks consisting of coaxial cables (annular waveguides) connected by T-joints. The spectra of the networks were measured in the frequency range 0.0001–16 GHz in order to obtain their statistical properties such as the integrated nearest neighbor spacing (INNS) distribution and the spectral rigidity $\Delta_3(L)$. The comparison of our experimental and theoretical results shows that microwave networks can simulate quantum graphs with time reversal symmetry (TRS). In particular, we use the spectra of the microwave networks to study the periodic orbits of the simulated quantum graphs. We also present experimental study of directional microwave networks consisting of coaxial cables and Faraday isolators for which the time reversal symmetry is broken. In this case our experimental results indicate that spectral statistics of directional microwave networks deviate from predictions of Gaussian orthogonal ensembles (GOE) in random matrix theory approaching, especially for small eigenfrequency spacing s , results for Gaussian unitary ensembles (GUE). Experimental results are supported by the theoretical analysis of directional graphs.

Quantum graphs of connected one-dimensional wires were introduced more than fifty years ago in order to describe organic molecules by free electron models [1, 2]. They can be considered as idealizations of physical networks in the limit where the widths of the wires are much smaller than their lengths, i.e. assuming that the propagating waves remain in a single transversal mode. Among the systems modeled by quantum graphs one can find e.g., electromagnetic optical waveguides [3, 4], quantum wires [5, 6], mesoscopic systems [7, 8] and excitation of fractons in fractal structures [9, 10]. In spite of the attention payed to quantum graphs, the statistical properties of their spectra were hardly investigated in the past. Recently spectral properties of quantum graphs have been studied in the series of papers by Kottos and Smilansky [11, 12, 13]. They have shown that quantum graphs are excellent paradigms of quantum chaos. However, in spite of numerous theoretical investigations of this topic [14, 15, 16, 17, 18, 19, 20, 21] no experiments have been performed so far.

The main aim of this work is to demonstrate that using a simple experimental setup consisting of microwave networks (throughout the text we also use the names: microwave graphs or circuits) one may successfully simulate quantum graphs. The circuits are constructed of coaxial cables (annular waveguides) connected by T-joints. Furthermore, to mimic the effects of the time reversal symmetry-breaking in quantum systems it is sufficient to add the Faraday isolators into the circuit.

The analogy between quantum graphs and microwave networks is based upon the equivalence of the Schrödinger equation describing the quantum system and the telegraph equation describing the ideal microwave circuit. It is worth noting that this paper continues the use of microwave spectroscopy to verify wave effects predicted on the basis of quantum physics, which for two-dimensional systems, thin microwave cavity resonators, was pioneered by [22] and further developed by [23, 24, 25, 26, 27, 28]. The first microwave experiment specifically devoted to study of quantum chaotic scattering was reported in [29]. Later on a similar experimental technique was applied in the observation of resonance trapping in an open microwave cavity [30]. In the case of two dimensions the Schrödinger equation for quantum billiards is equivalent to the Helmholtz equation for microwave cavities of corresponding shape. Three-dimensional chaotic billiards have been also studied experimentally in the microwave frequency domain [31, 32] but for these systems there is no direct analogy between the vectorial Helmholtz equation and the Schrödinger equation.

A general microwave graph consists of N vertices (T-joints in our case) connected by bonds e.g., coaxial cables. Following [12] we define the $N \times N$ connectivity matrix C_{ij} which takes the value 1 if the vertices i and j are connected and 0 otherwise. The coaxial cable consists of an inner conductor of radius r_1 surrounded by a concentric conductor of inner radius r_2 . The space between the inner and the outer conductors is filled with a homogeneous material having the dielectric constant ε . For frequency ν below the onset of the next TE_{11} mode [33], inside a coaxial cable can propagate only the fundamental TEM mode, in the literature often called a Lecher wave. This mode exists because the cross section of a coaxial line is doubly connected, what results in the existence of the potential difference between the inner and the outer conductors (see Eq. (2)).

In order to find propagation of a Lecher wave inside the coaxial cable joining the i -th and the j -th vertex of the microwave graph we can begin with the continuity equation for the charge and the current on the considered cable (bond) [34]

$$\frac{de_{ij}(x, t)}{dt} = -\frac{dJ_{ij}(x, t)}{dx}, \quad (1)$$

where $e_{ij}(x, t)$ and $J_{ij}(x, t)$ are the charge and the current per unit length on the surface of the inner conductor of a coaxial cable.

For the potential difference we can write down

$$U_{ij}(x, t) = V_2^{ij}(x, t) - V_1^{ij}(x, t) = \frac{e_{ij}(x, t)}{\mathcal{C}}, \quad (2)$$

where $V_1^{ij}(x, t)$ and $V_2^{ij}(x, t)$ are the potentials of the inner and the outer conductors of a coaxial cable and \mathcal{C} is the capacitance per unit length of a cable.

Taking the spatial derivative of (2) and assuming that the wave propagating along the cable is monochromatic $e_{ij}(x, t) = e^{-i\omega t}e_{ij}(x)$ and $U_{ij}(x, t) = e^{-i\omega t}U_{ij}(x)$ one can obtain [34]

$$\frac{d}{dx}U_{ij}(x) = -\mathcal{Z}J_{ij}(x), \quad (3)$$

where $\mathcal{Z} = \mathcal{R} - \frac{i\omega\mathcal{L}}{c^2}$. \mathcal{R} and \mathcal{L} denote the resistance and the inductance per unit length, respectively. The angular frequency ω is equal to $2\pi\nu$ and c stands here for the speed of light in a vacuum.

Making use of the equations (1-3) and the definition of \mathcal{Z} for an ideal lossless coaxial cable with the resistance $\mathcal{R} = 0$, one can derive the telegraph equation on the microwave

graph

$$\frac{d^2}{dx^2}U_{ij}(x) + \frac{\omega^2\varepsilon}{c^2}U_{ij}(x) = 0, \quad (4)$$

where $\varepsilon = \mathcal{LC}$ [35].

The continuity equation for the potential difference requires that for every $i = 1, \dots, N$

$$U_{ij}(x)|_{z=0} = \varphi_i, \quad U_{ij}(x)|_{z=L_{ij}} = \varphi_j, \quad i < j, \quad C_{ij} \neq 0. \quad (5)$$

The current conservation condition

$$\sum_{j<i} C_{ij} J_{ji}(x)|_{x=L_{ij}} - \sum_{j>i} C_{ij} J_{ij}(x)|_{x=0} = 0 \quad (6)$$

may be transformed using Eq. (3) into

$$-\sum_{j<i} C_{ij} \frac{d}{dx} U_{ji}(x)|_{x=L_{ij}} + \sum_{j>i} C_{ij} \frac{d}{dx} U_{ij}(x)|_{x=0} = 0, \quad (7)$$

where L_{ij} represents the length of the bond joining the i -th and the j -th vertex of the graph. To simplify the notation, the lengths of six bonds of the four-vertex graph shown in Figure 1 are labeled by letters $\{a, \dots, f\}$.

Assuming the following correspondence: $\Psi_{ij}(x) \Leftrightarrow U_{ij}(x)$ and $k^2 \Leftrightarrow \frac{\omega^2\varepsilon}{c^2}$, equation (4) is formally equivalent to the one-dimensional Schrödinger equation (with $\hbar = 2m = 1$) on the graph with the magnetic vector potential $A_{ij} = 0$ [12],

$$\frac{d^2}{dx^2}\Psi_{ij}(x) + k^2\Psi_{ij}(x) = 0. \quad (8)$$

It is easy to verify that equations (5) and (7) are equivalent to equations derived in [12] (see Eqs. (3)) for quantum graphs with Neumann boundary conditions ($\lambda_i = 0$) and vanishing magnetic vector potential $A_{ij} = A_{ji} = 0$. Such systems possess the time reversal symmetry (TRS),

$$\left\{ \begin{array}{l} \Psi_{ij}(x)|_{x=0} = \varphi_i, \quad \Psi_{ij}(x)|_{x=L_{ij}} = \varphi_j, \quad i < j, \quad C_{ij} \neq 0 \\ -\sum_{j<i} C_{ij} \frac{d}{dx} \Psi_{ji}(x)|_{x=L_{ij}} + \sum_{j>i} C_{ij} \frac{d}{dx} \Psi_{ij}(x)|_{x=0} = 0. \end{array} \right. \quad (9)$$

In order to check the equivalence of microwave and quantum graphs we measured the spectra of ten tetrahedral microwave graphs in the frequency range 0.0001 – 16 GHz. For

this frequency range only a Lecher wave can propagate in the graphs. The next mode to propagate is the TE_{11} with the cut-off frequency $\nu_c \simeq \frac{c}{\pi(r_1+r_2)\sqrt{\varepsilon}} = 32.9$ GHz [33], where $r_1 = 0.05$ cm is the inner wire radius of the coaxial cable (SMA-RG402), while $r_2 = 0.15$ cm is the inner radius of the surrounding conductor, and $\varepsilon = 2.08$ is Teflon dielectric constant.

The experimental set-up for measurements of spectra of the microwave graphs is shown in Figure 1. We used Hewlett-Packard 8672A microwave synthesizer to measure the spectra of the graphs in the frequency range 2 - 16 GHz while for the frequency range 0.0001 - 3 GHz Rhode-Schwartz SMT-03 microwave synthesizer was used. The microwave coupler (Narda 4055) enabled us to observe signals reflected from microwave graphs. Because for the specified frequency range only a single TEM mode could propagate in the microwave networks a reflected signal was proportional to $|S|^2$, where the complex number S may be considered as a one-dimensional scattering matrix. This type of microwave experiments, related to scattering matrix measurements, was pioneered by [29] and stimulated by [36]. In Figure 2(a) a typical fragment of a measured modulus of scattering matrix $|S|$ of the graph is presented in the frequency range 3.95 - 5.05 GHz. The experimental spectrum is also compared with numerically calculated eigenfrequencies of the ideal graph ($R = 0$) having the same bonds lengths as the experimental one. The total “optical” lengths of the microwave graphs, including T-joints, varied from 171.7 to 262.2 cm, which allowed for the observation of 156-264 eigenfrequencies in the frequency range 0.0001 - 16 GHz. To avoid the degeneracy of eigenvalues the lengths $L_{i,j}$ of the bonds (cables) were chosen not to be commensurable. The transmission through the T-joints was characterized by the weak frequency dependence e.g. in the frequency range 0.05 -16 GHz the ratio $R_S = (|S_{ij}|^{max} - |S_{ij}|^{min})/|S_{ij}|^{max} \leq 0.06$, where $|S_{ij}|^{max}$ and $|S_{ij}|^{min}$ are the maximum and the minimum values of modulus of non-diagonal elements of a three port scattering matrix S_{ij} , respectively. The indices $i, j = 1, 2, 3$ and $i \neq j$. For the frequency range 3.95-5.05 GHz specified in Figure 2(a) the ratio fulfilled the condition $R_S \leq 0.02$.

For more comprehensive comparison of the experimental and numerical results the experimental spectrum shown in Figure 2(a) is compared in Figure 2(b) with the response function $r(k)$ calculated for the graph having the same bonds lengths as the experimental one. The response function $r(k)$ was introduced in this paper in order to analyze the directional graphs consisting of Faraday isolators and is defined by Eq. (19). In the calculations of the response function $r(k)$ absorption of microwave cables were taken into account by

replacing the real wave vector k by the complex vector $k + i\beta\sqrt{k}$ [35]. The absorption coefficient $\beta = 0.009 \text{ m}^{-1/2}$ was evaluated on the basis of absorption of the microwave cables used in the experiment. The direct comparison of the results presented in Figure 2(a) and Figure 2(b) requires some care because the response function $r(k)$ is rather proportional to the amplitude of the field transmitted through the graph than to the amplitude reflected from the graph that is represented by the scattering matrix $|S|$. However, the aim of this comparison is to show that the inclusion of absorption of microwave cables leads to comparable with the experimental results broadening of resonances. It is also important noting that calculated in such a way eigenfrequencies are very close to the ones calculated for the ideal graph, from which they differ at most by 1 MHz. Figures 2(a-b) show that the agreement between experimental and theoretical results is quite good (the relative errors are of the order of 10^{-3}), what justifies a posteriori our assumption that the microwave circuits can be described with good accuracy by the quantum graphs with Neumann boundary conditions. In this way our experimental results additionally support theoretical findings about the boundary conditions for shrinking domains [37, 38]. Our results also show that relatively short microwave graphs consisting of coaxial cables, at least as it concerns the eigenvalues positions, can be approximately treated as ideal lossless graphs with the resistance $\mathcal{R} = 0$. The last statement is not very surprising. A similar situation one can find in the experiments with microwave cavities [22]. A thorough discussion on influence of absorption of energy caused by the finite conductivity of the cavity walls on reflected from the cavity power was given by Doron et al [29]. They showed (see also [30]) that small absorption of energy is necessary for revealing cavity's resonances as dips in the reflected power.

We have examined statistical properties of spectra of the microwave graphs such as the integrated nearest neighbor spacing (INNS) distribution $I(s)$ and the spectral rigidity $\Delta_3(L)$. (for their definitions see eg. [39, 40]). Figure 3 presents the INNS distributions. The solid line represents predictions of random matrix theory obtained for Gaussian Orthogonal Ensemble (GOE), applicable for systems with a time-reversal symmetry. The dashed line denotes results characteristic of Gaussian Unitary Ensemble (GUE), used if the time reversal symmetry is broken [39]. Experimental curve (open triangles) was obtained by averaging over the set of 10 microwave graphs obtained by varying with the length of one bond, which provided us with the total of 2220 experimentally measured eigenfrequencies. Numerical curve (open circles) shows results averaged for ten quantum graphs having the same bonds

lengths as the experimental ones. Eigenfrequencies were calculated by solving numerically the secular equations for quantum graphs (Eqs. (6-8) in [12]). This procedure allowed us to identify total of 2344 eigenfrequencies, slightly more than measured experimentally. Figure 3 shows that in both cases the INNS distributions are in a very good agreement with the GOE predictions.

Figure 4 demonstrates the spectral rigidity $\Delta_3(L)$ obtained for the microwave graph of the “optical” length 223.6 cm. Experimental curve (open triangles) was based on 229 identified eigenfrequencies, while the numerical data (open circles) were computed out of 237 eigenfrequencies. In both cases the frequency range was 0.0001–16 GHz. Deviations of the experimental and numerical rigidity from the GOE predictions (solid line) are visible. For comparison the dashed line in Figure 4 shows the RMT prediction for GUE. Our experimental and numerical results are lying above the GOE prediction for L between 2.5 – 5. For higher value of L a saturation of the numerical value of the spectral rigidity is observed in agreement with the predictions of Berry [42]. The experimental rigidity for $L > 10$ is located below the GOE curve and above the numerical results. The departure of the experimental rigidity from the numerical one can be probably attributed to the loss of about 3% of experimental eigenfrequencies.

The measurements of the spectra of the graphs enabled us also to calculate the lengths of periodic orbits in the graph. They were computed from the Fourier transform

$$F(l) = \int_0^{k_{max}} \tilde{\rho}(k) \omega(k) e^{-ikl} dk, \quad (10)$$

where $\tilde{\rho}$ is the oscillating part of the level density and $\omega(k) = \sin^2(\pi \frac{k}{k_{max}})$ is a window function that suppresses the Gibbs overshoot phenomenon [28, 41]. Here k_{max} is the maximal value of the wave number within the interval where the eigenvalues of the graph were evaluated. In order to extract the oscillating part of the level density $\tilde{\rho}$ we determined the density of states according to $\rho(k) = \sum_j \delta(k - k_j)$ and subtracted from it the mean density $\bar{\rho}(k) = d\bar{N}(k)/dk$. The mean $\bar{N}(k)$ of the staircase function, i.e., the number of resonances up to the wave number k , was obtained from a least squares fit $\bar{N}(k) = \alpha_1 k + \alpha_2$ of the measured staircase $N(k)$. The slope parameter, obtained from the experimental data, $\alpha_1 = 0.707 \pm 0.006$, is very close to the value $\alpha = 0.712$, received from the Weyl formula given by Eq. (7) in [11].

The absolute square of the Fourier transform of the fluctuating part of the density of

resonances $|F(l)|^2$ for the graph of the “optical” length 223.6 cm is shown in Figure 5. The lengths of the bonds of this graph fulfill the following relations: $a < b < c < d < e < f$. Results obtained from the experimental spectrum (solid line) are compared to the results obtained from numerical calculations (dotted line). The experimental spectrum included 149 identified eigenfrequencies while the numerical one 150 eigenfrequencies. In both cases the frequency range was 0.2–10.2 GHz. We used the narrower frequency range than in the calculations of the INNS distributions and $\Delta_3(L)$ to be sure that at most only one eigenfrequency was missing in the experimental spectrum. The absolute square of the Fourier transform $|F(l)|^2$ shows pronounced peaks near the lengths of certain periodic orbits. The agreement between the experimental and the numerical results is good, however, some discrepancies for shorter periodic orbits are visible. In Figure 5 we show all irreducible periodic orbits [12], i.e. periodic orbits which do not intersect themselves, with the lengths $l < 165$ cm. For clarity, in Figure 5 we additionally show the first repetition of the periodic orbit $2b$ at $l = 2b + 2b = 105.2$ cm and two reducible periodic orbits $abc + 2c$ and $bde + 2a$ at $l = 149.3$ cm and $l = 154.7$ cm, respectively. It should be noticed that many peaks for $l > 70$ cm cover several unresolved periodic orbits. In order to check whether the missed resonance was responsible for discrepancies in the lengths of periodic orbits we artificially added this resonance to the spectrum of the graph and recalculated the lengths of periodic orbits (results are not shown). Indeed, the inclusion of the missed level improved the agreement with the numerical results. The main change was visible in the ”experimental” amplitudes that became closer to the numerical ones. For example the amplitudes of the most sensitive orbits $2a$ and $2b$ (see Fig. 5) were decreased from 1.5 to 1.0 and from 1.4 to 1.1, respectively. The positions of the periodic orbits were not as sensitive as amplitudes. For example in the case of the orbit $2a$ the length was changed from $\ell = 42.0$ cm to $\ell = 41.4$ cm becoming more distant from the numerical result $\ell = 42.0$ cm. In a different way behaved the orbit $2b$ which length was modified from $\ell = 51.5$ cm to $\ell = 52.5$ cm becoming closer to the numerical result $\ell = 52.6$ cm.

In this paper we also present experimental study of microwave graphs consisting of coaxial cables and Faraday isolators. The graphs with Faraday isolators are examples of simple experimental realization of directional graphs for which the time reversal symmetry is broken. A microwave Faraday isolator is a passive device, which transmits the wave moving in one direction while absorbing the wave moving in the opposite direction. Due to absorption

the introduction of Faraday isolators transforms the problem from the bound system to an open system. In the experiment AerCom 60583 Faraday isolators (insertion loss < 0.4 dB, isolation > 19 dB, length = 5.7 cm) with the operating frequency range 3.5 – 7.5 GHz were used. We measured the spectra of four graphs consisting in one of their bonds one Faraday isolator or two Faraday isolators connected in series. The limitations imposed by the narrow range of isolators operating frequency lead to rather poor eigenfrequencies statistics - between 34 and 39 eigenfrequencies were observed for the graphs with Faraday isolators. Therefore, for each of four graphs we performed three measurements where: the isolator was mounted in the bond b of the graph, the isolator was mounted in the bond d , and two isolators connected in series were mounted in the bond d . The assignment of the letters to the bonds of the graph is shown in Figure 1.

The results of these twelve measurements (together 444 eigenfrequencies) were averaged to obtain the INNS distribution (solid triangles in Figure 6). The INNS distribution obtained for the same frequency range, but without Faraday isolators are also shown in Figure 6 (open triangles). The examination of the INNS distribution obtained for the graphs, with and without Faraday isolators, shows that they are different. In spite of some deviations, one can see that INNS distribution for the graphs without the isolators is close to the RMT prediction for GOE (solid line) in contrast to the INNS distribution for the graphs with the isolators, which follows more closely the RMT prediction for GUE (dashed line). This is especially well seen at small eigenfrequency spacing s . Similar deviations of the spectral statistics were reported by experiments with microwave billiards [25, 26, 27]. In the experiment performed by So et al. [25] the transition from GOE to GUE statistics was caused by a piece of magnetized ferrite placed inside a two-dimensional microwave cavity while in the experiment performed in Marburg [26, 27] the deviation from GOE statistics was induced by Faraday isolator connected to a microwave cavity.

The directed graphs can be also modeled theoretically. The crucial element of the graph — the Faraday isolator in a directed bond — can be described by means of a filter factor which damps the wave moving in one direction. In the numerical analysis of the directed graphs we have assumed that measuring the reflection spectra of the graphs we are rather probing the graphs as closed systems by some coupling, which is weak enough, not to influence the internal dynamics of the systems.

We introduce the connectivity matrix D of a directed graph, which does not need to be

symmetric. With any directed graph Γ one may associate a bidirectional graph G with the same number of vertices. Its connectivity matrix C is symmetric,

$$C_{ij} = \max(D_{ij}, D_{ji}). \quad (11)$$

The number B of bonds in the graph G is equal to $B = \frac{1}{2} \sum_{ij} C_{ij}$. To be able to filter some waves propagating in one direction while preserving those moving in the opposite direction we will use a bond scattering technique of analyzing spectra of graphs, similar to this introduced by Kottos and Smilansky [12]. Consider a plain wave $\Psi_{j'n}(x) = e^{-ikx}$ coming from the vertex j' to the vertex n . It is scattered into all bonds going out from the vertex n , for which $C_{nj} \neq 0$,

$$\Phi_{nj}(x) = \delta_{jj'} e^{-ikx} + \sigma_{jj'}^{(n)} e^{ikx}. \quad (12)$$

The vertex scattering matrix $\sigma_{jj'}^{(n)}$ is completely determined, if we assume Neumann boundary conditions (9), which imply

$$\sigma_{jj'}^{(n)} = C_{j'n} C_{nj} (-\delta_{jj'} + 2/v_n). \quad (13)$$

Here v_n denotes the number of bonds meeting at the n -th vertex, also called the *valency* of the vertex. Elements of $\sigma_{jj'}^{(n)}$ for all vertex n combine to the entire bond transition matrix of the graph G

$$T_{jl,nm} = \delta_{ln} C_{jl} C_{nm} \sigma_{jm}^{(l)}, \quad (14)$$

which describe the changes of amplitudes of waves propagating in each bond of the graph (in both directions) after one event of scattering on vertices. The matrix dimension is equal to twice the number of bonds B in the graph. To take into account the presence of the Faraday isolators we make use of the connectivity matrix D of the directed graph Γ , and introduce a diagonal $2B \times 2B$ matrix $\Lambda(k)$

$$\Lambda_{jl,j'l'}(k) = \delta_{jj'} \delta_{ll'} D_{jl} e^{ikL_{jl}}, \quad (15)$$

where the phase factor describes the free propagation along the bond (jl) of length L_{jl} . By definition, the element D_{jl} is equal to zero for bonds which do not belong to the directed graph Γ . The effect of absorption of the microwave field by microwave cables can be easily taken into account by modifying the matrix $\Lambda_{jl,j'l'}(k)$ given by Eq. (15) to the form

$\delta_{jj'}\delta_{ll'}D_{jl}e^{(ik-\beta\sqrt{k})L_{jl}}$, where β is the absorption coefficient. The total evolution of the vector of wave amplitudes of length $2B$ is given by the bond scattering matrix

$$S(k) = \Lambda(k) \cdot T. \quad (16)$$

The matrix $S(k)$ is sub-unitary, since it is obtained by putting to zero some elements of a unitary matrix. We denote the eigenvalues of $S(k)$ by $\lambda_j(k)$, all of $\lambda_j(k)$ are located in (or at) the unit circle, $|\lambda_j(k)| \leq 1$. The equation for the eigenmodes of the quantum graph

$$\det(S(k) - 1) = 0 \quad (17)$$

may have no real solution. In our experimental setup the graph is driven by the microwave generator. We are interested, for which wave vectors k the resonant driving of the graph will appear. We analyze the stationary state of the system, in which an arbitrary number p of scattering processes take place and decompose it in the eigenbasis of $S(k)$. The amplitudes of each mode become an infinite superposition of waves scattered p times, so the enhancement factor $r_j(k)$ of the j -th mode reads

$$r_j(k) = \sum_{p=0}^{\infty} [\lambda_j(k)]^p = \frac{1}{1 - \lambda_j(k)}, \quad (18)$$

where $\lambda_j(k)$ are the eigenvalues of the bond scattering matrix $S(k)$. Since each eigenmode may contribute to the resonant dissipation in the system, we approximate the total response function of the graph by the average enhancement factor (the mean of $r_j(k)$)

$$r(k) = \frac{1}{2B} \sum_{j=1}^{2B} r_j(k) = \frac{1}{2B} \sum_{j=1}^{2B} \frac{1}{1 - \lambda_j(k)}. \quad (19)$$

Maxima of this function, which occur if one of the eigenvalue $\lambda_j(k)$ is close to unity, identify resonant values of the wave vector k . We analyzed the function $r(k)$ generated for parameters of the system as used in the experiment and studied numerically the statistics of its maxima.

Using this approach we calculated approximated eigenfrequencies of twenty directed graphs in the frequency range 0–20 GHz. As in the experimental realization, only one bond was assumed to be directed. Numerical search for the eigenfrequencies was performed for two sets of directed graphs with five different lengths of a directed bond b (see Figure 1 for the assignment of the letters to the bonds of the graph). The other bonds of the graphs were bidirectional and within the set were kept fixed. The same number of numerical calculations were also done for two sets of directed graphs with the varied length of the directed

bond d . Figure 7 shows the integrated nearest neighbor spacing distribution averaged for twenty realizations of the directed graphs in the frequency range 0 – 20 GHz. Together 3207 eigenfrequencies were used in the calculations of the INNS distribution. In this case we decided not to put the experimental and theoretical data on one plot, to emphasize that the results are based on different statistics and cannot be directly compared. However, it is justified to compare these numerical results obtained for the directed graphs (solid circles) with the numerical data obtained in the frequency range 0 – 20 GHz for twenty realizations of standard (bidirectional) graphs (empty circles). In this case 4641 eigenfrequencies were used in the calculations of the INNS distribution. Theoretical predictions for GOE and GUE, denoted by solid and dashed curve, respectively, suggest that the INNS spectral statistics for directed graphs deviate at small spacings from the GOE curve and become closer to the GUE predictions. This result confirms also our experimental findings for the microwave directed graphs.

In summary, we show that quantum graphs with Neumann boundary conditions can be simulated experimentally by microwave networks. Bidirectional microwave graphs, i. e. circuits without Faraday isolators, simulate quantum graphs with time reversal symmetry. The results for the directional microwave graphs with Faraday isolators, for which the time reversal symmetry is broken, indicate that their certain characteristics such as the integrated nearest neighbor spacing distribution can significantly differ from the RMT prediction for GOE, approaching the results characteristic of GUE.

Acknowledgments. This work was partially supported by KBN grants No 2 P03B 023 17 and 2 P03B 047 27. We would like to thank Professors Marek Kuś and Petr Šeba for valuable discussions.

-
- [1] L. Pauling, J. Chem. Phys. **4**, 673 (1936).
 - [2] H. Kuhn, Helv. Chim. Acta, **31**, 1441 (1948).
 - [3] C. Flesia, R. Johnston, and H. Kunz, Europhys. Lett. **3**, 497 (1987).
 - [4] R. Mitra and S. W. Lee, *Analytical techniques in the Theory of Guided Waves* (Macmillan, New York, 1971).
 - [5] E. L. Ivchenko, A. A. Kiselev, JETP Lett. **67**, 43 (1998).

- [6] J.A. Sanchez-Gil, V. Freilikher, I. Yurkevich, and A. A. Maradudin, Phys. Rev. Lett. **80** , 948 (1998).
- [7] Y. Imry, *Introduction to Mesoscopic Systems* (Oxford, New York, 1996).
- [8] D. Kowal, U. Sivan, O. Entin-Wohlman, Y. Imry, Phys. Rev. B **42**, 9009 (1990).
- [9] Y. Avishai and J.M. Luck, Phys. Rev. B **45**, 1074 (1992).
- [10] T. Nakayama, K. Yakubo, and R. L. Orbach, Rev. Mod. Phys. **66**, 381 (1994).
- [11] T. Kottos and U. Smilansky, Phys. Rev. Lett. **79**, 4794 (1997).
- [12] T. Kottos and U. Smilansky, Annals of Physics **274**, 76 (1999).
- [13] T. Kottos and U. Smilansky, Phys. Rev. Lett. **85**, 968 (2000).
- [14] T. Kottos and H. Schanz, Physica E **9**, 523 (2003).
- [15] T. Kottos and U. Smilansky, J. Phys. A **36**, 3501 (2003).
- [16] F. Barra and P. Gaspard, Journal of Statistical Physics **101**, 283 (2000).
- [17] G. Tanner, J. Phys. A **33**, 3567 (2000).
- [18] G. Tanner, J. Phys. A **34**, 8485 (2001).
- [19] P. Pakoński, K. Życzkowski and M. Kuś, J. Phys. A **34**, 9303 (2001).
- [20] P. Pakoński, G. Tanner and K. Życzkowski, J. Stat. Phys. **111**, 1331 (2003).
- [21] R. Blümel, Yu Dabaghian, and R.V. Jensen, Phys. Rev. Lett. **88**, 044101 (2002).
- [22] H.J. Stöckmann and J. Stein, Phys. Rev. Lett. **64**, 2215 (1990).
- [23] S. Sridhar, Phys. Rev. Lett. **67**, 785 (1991).
- [24] H. Alt, H.-D. Gräf, H. L. Harner, R. Hofferbert, H. Lengeler, A. Richter, P. Schardt, and A. Weidenmüller, Phys. Rev. Lett. **74**, 62 (1995).
- [25] P. So, S. M. Anlage, E. Ott, and R. N. Oerter, Phys. Rev. Lett. **74**, 2662 (1995).
- [26] U. Stöffregen, J. Stein, H.-J. Stöckmann, M. Kuś, and F. Haake, Phys. Rev. Lett. **74**, 2666 (1995).
- [27] F. Haake, M. Kuś, P. Šeba, H.-J. Stöckmann, and U. Stöffregen, J. Phys. A **29**, 5745 (1996).
- [28] L. Sirko, P. M. Koch, and R. Blümel, Phys. Rev. Lett. **78**, 2940 (1997).
- [29] E. Doron, U. Smilansky, and A. Frenkel, Phys. Rev. Lett. **65**, 3072 (1990).
- [30] E. Persson, I. Rotter, H.-J. Stöckmann, and M. Barth **85**, 2478 (2000).
- [31] S. Deus, P. M. Koch, and L. Sirko, Phys. Rev. E **52**, 1146 (1995).
- [32] C. Dembowski, B. Dietz, H.-D. Gräf, A. Heine, T. Papenbrock, A. Richter, and C. Richter, Phys. Rev. Lett. **89**, 064101-1 (2002).

- [33] D. S. Jones, *Theory of Electromagnetism* (Pergamon Press, Oxford, 1964), p. 254.
- [34] L.D. Landau, E.M. Lifshitz, *Electrodynamics of Continuous Media* (Pergamon Press, Oxford, 1960).
- [35] G. Goubau, *Electromagnetic Waveguides and Cavities* (Pergamon Press, Oxford, 1961).
- [36] R. Blümel and U. Smilansky, Phys. Rev. Lett. **60**, 477 (1988).
- [37] P. Kuchment, H. Zeng, J. Math. Anal. Appl. **258**, 671 (2001).
- [38] J. Rubinstein, M. Schatzman, Arch. Rat. Mech. Anal. **160**, 271 (2001).
- [39] F. Haake *Quantum Signatures of Chaos* (II ed. Springer, Berlin, 2000).
- [40] H.-J. Stöckmann *Quantum Chaos - An Introduction* (Cambridge University Press, Cambridge, 1999).
- [41] Sz. Bauch, A. Błędowski, L. Sirko, P. M. Koch, and R. Blümel, Phys. Rev. E **57**, 304 (1998).
- [42] M.V. Berry, Proc. R. Soc. London A **400**, 229 (1985).

FIG. 1: Experimental set-up for measurements of the spectra of the microwave graphs. Microwave synthesizer: HP8672A (2-18.5 GHz) and SMT03 (5 kHz-3 GHz), D - crystal detector (HP8472B), C - microwave coupler (Narda 4055).

FIG. 2: (a) A fragment of a measured modulus of scattering matrix $|S|$ of the microwave graph of the “optical” length 223.6 cm in the frequency range 3.95–5.05 GHz. (b) The response function $r(k)$ calculated for the graph having the same bonds lengths as the experimental one. In the calculations of the response function $r(k)$ absorption of the microwave field by coaxial cables were taken into account (see text). Vertical broken lines show the positions of numerically calculated eigenfrequencies of the graph without absorption.

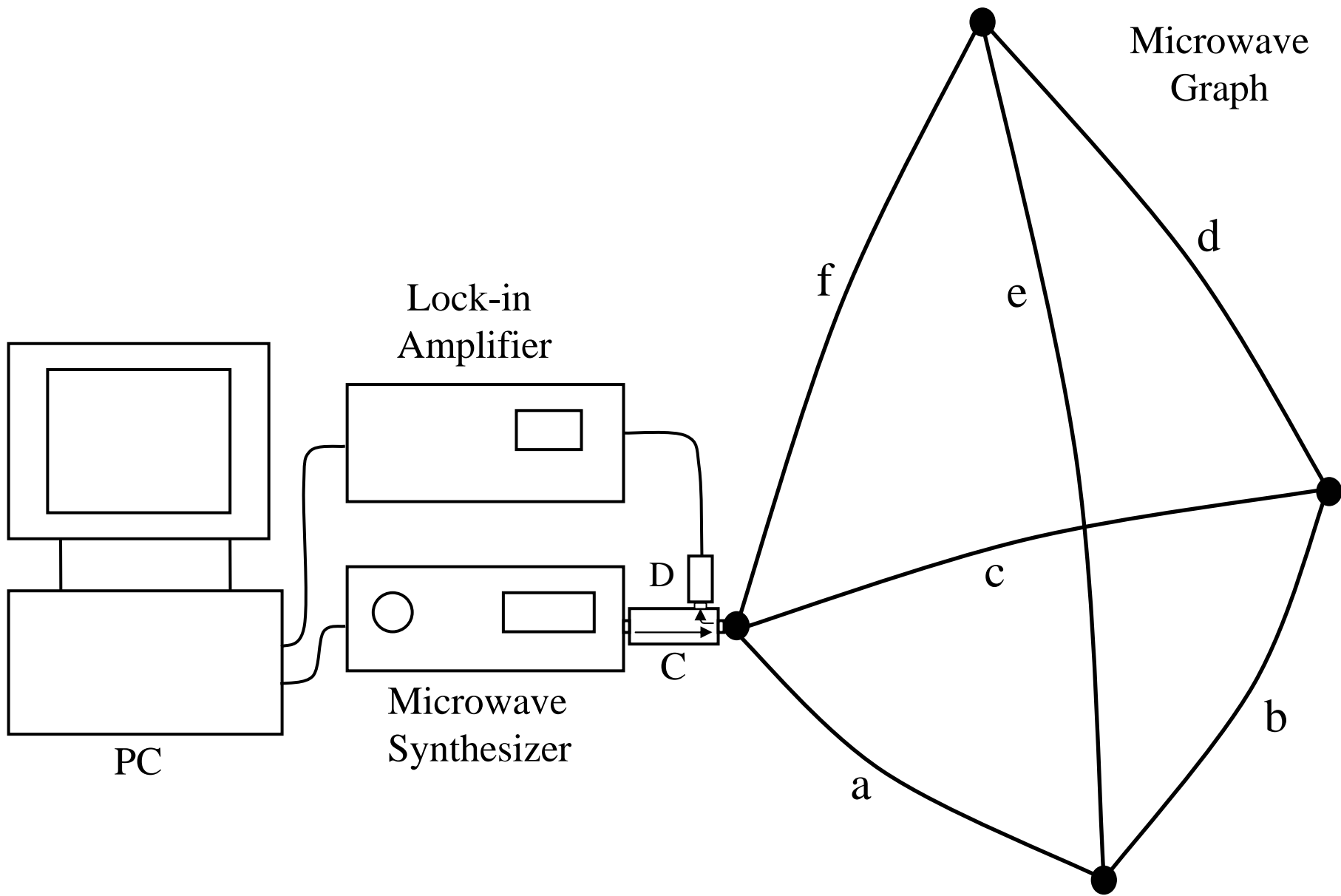
FIG. 3: Integrated nearest neighbor spacing (INNS) distribution $I(s)$ averaged for 10 microwave graphs. Results of the experiment (open triangles) are compared with the numerical results (open circles) and theoretical prediction for GOE (solid line) and GUE (dashed line).

FIG. 4: Spectral rigidity $\Delta_3(L)$ for the microwave graph of the “optical” length 223.6 cm. Results of the experiment (open triangles) are compared with the numerical results (open circles) and theoretical prediction for GOE (solid line) and GUE (dashed line).

FIG. 5: Absolute square of the Fourier transform of the fluctuating part of the density of resonances of the graph of the “optical” length 223.6 cm. Results of the experiment (solid line) are compared with the numerical results (dotted line). The assignment of peaks of $|F(l)|^2$ to simple periodic orbits (see text) is shown along with the length of the orbits. The “optical” lengths of the bonds of the graph: $a = 21.0$ cm, $b = 26.3$ cm, $c = 34.0$ cm, $d = 39.6$ cm, $e = 46.8$ cm, $f = 55.9$ cm.

FIG. 6: Integrated nearest neighbor spacing distribution averaged for eight realizations of the microwave graphs with Faraday isolators (solid triangles) is compared with the averaged results for the microwave graphs without the isolators (open triangles) and theoretical prediction for GOE (solid line) and GUE (dashed line). In both cases experimental results were obtained for the frequency range 3.5 – 7.5 GHz.

FIG. 7: Numerically calculated integrated nearest neighbor spacing (INNS) distributions averaged for twenty realizations of the directed graphs (solid circles) is compared with the averaged results for the bidirectional graphs (open circles). Calculations were performed in the frequency range 0 – 20 GHz. Numerical results for the INNS distributions are compared with theoretical predictions for GOE (solid line) and GUE (dashed line).



PC

Microwave
Synthesizer

Lock-in
Amplifier

Microwave
Graph

C

D

f

e

d

c

a

b

